Soft Matter RSCPublishing

ARTICLE

Structural determinants in a library of low molecular weight gelators

Cite this: DOI: 10.1039/x0xx00000x

Kyle L. Morris,[a,b] Lin Chen,[c] Alison Rodger,[b] Dave J. Adams[c] and Louise C. Serpell[a*]

Received ooth January 2014,
Accepted ooth January 2014

DOI: 10.1039/x0xx00000x

www.rsc.org/

Low molecular weight hydrogels are formed by molecules that form a matrix that immobilises water to form a self-supporting gel. Such gels have uses as biomaterials such as molecular scaffolds and structures for tissue engineering. One class of low molecular weight gelators (LMWG), naphthalene-conjugated dipeptides, has been shown to form hydrogels via self-assembly following a controlled drop in pH. A library of naphthalene-dipeptides has been generated previously although the relationship between the precursor sequence and the resulting self-assembled structures remained unclear. Here, we have investigated the structural details of a set of dipeptide sequences containing alanine (A) and valine (V) conjugated to naphthalene groups substituted with a Br, CN or H at the 6-position. Electron microscopy, circular dichroism and X-ray fibre diffraction shows that these LMWG may be structurally classified by their composition: the molecular packing is determined by the class of conjugate, whilst the chirality of the self-assemblies can be attributed to the dipeptide sequence. This provides insights into the relationship between the precursor sequence and the macromolecular and molecular structures of the fibres that make up the resulting hydrogels.

Introduction

The formation of hydrogels from low molecular weight gelators (LMWG) is a useful route to the production of materials for a wide range of applications.[1, 2] A recent expansion in the number of LMWG systems reported has led to a rapid growth in reports of characterisation and applications of a particular class of this type of molecule, namely aromatic conjugated dipeptide LMWG.[3-8] These systems typically consist of a hydrophobic, often aromatic, dipeptide sequences conjugated to Fmoc (9-fluorenylmethoxycarbonyl) [9, 10] or naphthalene [3, 4]; further conjugations have also been reported.[11, 12] Through the use of an environmental cue,[13] such as an enzymatic trigger,[14] temperature,[15, 16] or light[12] some of these conjugates self-assemble into anisotropic fibrils that can eventually cause hydrogelation through the immobilisation of water by the fibrillar network. There are now a large number of systems reported in the literature.[17] It is apparent from previous work that two LMWG molecules that differ only by a single amino acid can give rise to hydrogels with dramatically different rheological and phase properties.[3, 4, 10, 18] However, the structural basis for these differences in material properties is not understood.

The short-range molecular architecture of some LMWG systems has been studied. For example, the chirality of assembled naphthalene conjugated dipeptides has been reported to correlate to the D- or L-enantiomer of the incorporated amino acids with left- and right-handed assemblies being formed respectively.[3] Other reports have indicated that proteinaceous additives induce changes to the chiral organisation of the self-assembled hydrogelating molecules.[19] In addition to the plethora of molecular hydrogels with varying material properties available, the morphology of the constituent fibrils making these gels is reported to vary extensively: fibrils, laterally associated fibrils, helical-ribbons, ribbons and tapes, and nanotubes have all been reported to result from the assembly of peptidic LMWG.[20-23] It is known that the self-assembled structures for these classes of molecule are often stabilised by extended hydrogen bonded networks of ß-strands and π-π aromatic interactions.[3, 20, 22, 24] Despite the limited range of non-covalent stabilising interactions, these molecules have access to a large and elaborate range of supramolecular structures which give rise to variable morphologies, presumably due to the large degrees of freedom available in three-dimensional packing motifs and subtle difference in the energies of intermolecular interactions. It has been suggested that particular molecular structures may give rise to a pre-

determined morphology which would, in turn, have a predictable impact on the properties of subsequent rheological properties of the hydrogel formed.[20] However, the relationship between precursor composition, assembly conditions, and self-assembled structure remains unclear. Further, it is becoming increasingly clear that kinetics and the assembly process play a significant role in the outcome of the gelation, and hence the mechanical properties of the final gels.[8] An increased knowledge of how precursor design relates to self-assembled structure would not only represent a significant advance in scientific understanding of the self-assembly, but could potentially enable the rational design of fibril morphology and perhaps hydrogel material properties.

Attempts to identify molecular structure–property relationships have so far characterised aspects of the molecular architectures of dipeptide self-assembled fibrils using methods such as computational structure prediction, powder diffraction (pXRD), X-ray crystallography, wide angle X-ray scattering (WAXS) and X-ray fibre diffraction (fXRD).[3, 20, 22] Each of these techniques has revealed a great deal of structural information on the systems studied. However, as shown by Adams et al., whilst the crystalline phase of LMWG assemblies is related to computational structure predictions, the structure of final fibre phase for these systems remains elusive.[18, 25] It is apparent that crystals and fibres have structural features in common, but also show fundamental differences.[25] For investigations relevant to the gel phase, it is essential to interrogate the structure of self-assembled LMWG in the fibre phase. We have previously reported on the detailed structural characterisation of two LMWG systems in the assembled fibrillar phase[20, 25] benefitting from the additional directional information granted by fXRD and revealing a highly organised repetitive arrangement of the molecules along the fibre axis.

Here, we have investigated a set of dipeptide sequences containing alanine (A) and valine (V) conjugated to naphthalene (Nap) groups containing Br, CN or H to probe the contribution of different parts of the molecule to the structural architectures. Whilst we have detailed the gelation ability of this library previously,[26] we have not discussed the effect of peptide sequence and substituents on the molecular packing of the LMWG. We report on their structure in the fibrillar phase using electron microscopy, Fourier transform infrared spectroscopy (FTIR) and circular dichroism (CD) to probe secondary structure and chirality, and fXRD to determine their molecular packing.

Results and discussion

Construction of a low molecular weight gelator library

A set of dipeptide, naphthalene-based LMWG were synthesized as previously described [26] and are shown in Figure 1. Full characterisation data can be found elsewhere.[26] Gelation was induced using the well-characterised hydrolysis of glucono-δ-lactone (GdL) to gluconic acid to provide a controlled reproducible gelation.[13] The assembled structures were subjected to a range of morphological and biophysical analyses. We have previously shown that the pK_a of this family of gelators is affected by the hydrophobicity of the dipeptide.[26] This directly influences the pH at which the samples form gels. As we vary the structure in this series, the overall hydrophobicity and hence pH at which gels are formed changes. However, once gels are formed, these are stable at a lower pH than that at which the gel is formed. In this study, we have used a constant amount of GdL to adjust the pH. As such, all samples when studied (unless otherwise stated, after overnight gelation) are at a pH of 4.6. This value is sufficiently below the pK_a of all dipeptides in the series that direct comparison is valid. In all cases, a self-supporting gel was formed.

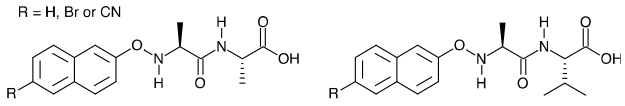

Figure 1. The generic chemical structure of the dipeptide LMWG forming the basis of the library by modification to positions C_6. Left is the alanine-alanine (AA) sequence, right is the alanine-valine (AV) sequence. The variants R at position C_6 are –H (naphthalene), -Br (bromonaphthalene) and –CN (cyanonaphthalene).

Fibrillar morphologies are adopted on self-assembly

Transmission electron microscopy (TEM) reveals the formation of self-assembled fibrils for all of the LMWG dipeptides following acidification, although their morphologies and lateral packing differ (Figure 2 and Supplementary Figure 1). Narrow filaments were observed for H-Nap-AA at ~7 nm whilst variably laterally associated fibrils of H-Nap-AV over a broad distribution of sizes formed. The tube-like structures (Figure 2c, arrows) observed for Br-Nap-AA have a broad distribution of sizes, the width of the bilateral structure measuring ~20 nm. Similar to H-Nap-AV, Br-Nap-AV adopted a broad distribution of fibril widths again with high levels of variable long-range lateral association. Some helical filaments were observed with variable helical parameters, in one instance (Figure 2d, arrow) having a width of 56 nm and a helical twist of 409 nm. CN-Nap-AA and CN-Nap-AV more consistently assemble into fibrils with a width of 14–15 nm, with clear regular twist and a rise of ~ 60 nm in each case.

Although H-Nap-AV is able to form crystals,[25] it formed hydrogelated, fibrillar morphologies under the conditions used here. Whilst the presence of fibrillar structures is consistent with our previous observations of the formation of gels,[20, 26] it is clear that there are differences in morphology between the different systems. Particularly interestingly, the morphological features could be classified according to whether the system possessed naphthalene, bromonaphthalene or cyanonaphthalene.

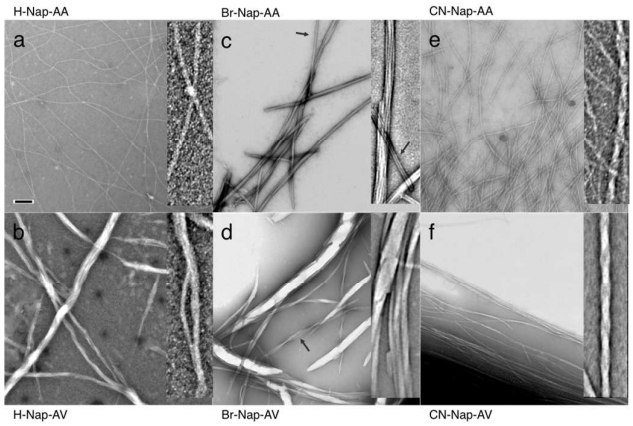

Figure 2. Transmission electron micrographs (TEM) of the aliphatic dipeptides (a) H-Nap-AA, (b) H-Nap-AV, (c) Br-Nap-AA, (arrows highlight individual filaments), (d) Br-Nap-AV, (e) CN-Nap-AA and (f) CN-Nap-AV. The black scale bar represents 200 nm for all micrographs. Insets highlight morphologies characteristic of each system (not to scale).

Where H is the substituent at C_6 on the naphthalene, narrow filaments were formed, whereas gelators with the bulky polarisable Br substituent gave laterally associated structures, as can be seen from the inset to Fig. 2c and d. Those with the CN group showed rope like, twisted fibrils. This indicates a role for the functional group on the naphthalene ring in determining the extent of lateral association and packing of individual protofilaments.

It should be noted that different morphologies have been reported for a range of related dipeptides, amino acid and dipeptide based gelators.[27-30] For example Ryan et al. have reported a series of Fmoc-amino acid gelators. Their TEM data suggested that one substitution position on the amino acid favoured bundling.[27-30] However, here we are able to correlate different behaviour depending on the aromatic ring at the N-terminus as opposed to the amino acids used.

Extended peptide conformation and naphthalene association drive self-assembly

FTIR spectra of the dipeptide gels revealed the self-assembled peptide secondary structure. Peaks were detected for all the dipeptides at approximately 1630 cm^{-1} indicating ß-sheet content (Table S1). The spectra also revealed an intense band at around 1650 cm^{-1} which is probably either due to random coil conformation [31] or an infrared stretching band of –C=C– on the naphthalene ring. This could potentially be attributed to the terminal amide group; interpreting these short dipeptides with N-protecting groups since using data from proteins or peptides is a challenge. This has also been suggested by others for related LMWG systems.[32]

No significant differences between the LMWG were detected by FTIR. Hence, in order to examine further the chiral characteristics of the hydrogelating systems, circular dichroism (CD) spectra were collected. Sampling from preformed gels was not able to effectively remove material for spectroscopic analysis, and so gelation was performed *in situ* and CD spectra collected after overnight incubation. This also enabled us to reliably subtract the relatively small but measureable CD signal from hydrolysed GdL. Figure 3 shows representative CD spectra for the dipeptide library. The signals characteristic of each system were found to develop over the course of self-assembly and hydrogelation (Supplementary Figure 2) and represent an elongation of the fibril structures within the gel. Previous studies have shown that CD spectra collected from fibrillar samples may exhibit LD artefacts as a result of fibril alignment.[33, 34] Cuvette rotation confirmed there was no significant directional signal dependence (LD) in any of the samples so the spectra are true CD spectra of the dipeptide self-assembled structures (Figure 3).

An isolated naphthalene chromophore exhibits absorbance signals from 200 – 230 nm (long axis polarized with maximum at 225 nm) and 240 – 290 nm (short axis polarized).[35] Any exciton coupling of the naphthalene chromophores will have a net hypochromic absorbance intensity and wavelength shift as well as leading to positive and negative components in CD spectra whose zero is at the absorbance maximum. The peptide chromophores' π-π* transitions are centered around 195 nm and the less intense n-π* transitions at 220 nm where substituents tend to shift transitions to longer wavelengths. However, the magnitude of the peptidic transitions are far weaker than the coupled transitions of the naphthalene moiety and so are hidden in the spectra shown in Figure 3.

The spectra are dominated by series of exciton couplets exclusively from the naphthalene groups (between (200 – 230 nm) as shown in Figure 3 (see also Supplementary Figure 2). By accounting for the contribution of light scattering from the background solvent (as described in the experimental section), the absorbance of the assemblies may be derived from HT[V] recordings (dotted lines and Supplementary Figure 4) and thus each exciton couplet observed in the CD may assigned to its respective absorption chromophore (Table 1 and Supplementary Table 2). The CN-Nap-AA CD signal intensities are significantly smaller and occur at the monomer transitions for naphthalene indicating less efficient exciton coupling and thus chiral order (Figure 3e). For this LMWG, in general the signals occur at the monomer transitions, indicating the naphthalene chromophores are not stacked efficiently in the final structures. This is an important point. Others have suggested that efficient stacking of the aromatic groups at the N-terminus of the dipeptide drives the assembly.[22] Our data strongly suggests otherwise for this LMWG that still self-assembles and forms a gel. In the other five dipeptides where exciton couplets associated with the naphthalene groups are observed, this indicates that the naphthalene chromophores are subject to highly organised chiral stacking, as previously observed.[20] The sign of the Cotton effect associated with each naphthalene exciton couplet indicates the handedness of the chiral arrangement is related to the dipeptide sequence. The peptide sequence determined the handedness: dipeptides with the sequence Ala-Val have a left-handed helical naphthalene arrangement and those with the sequence Ala-Ala have the converse right-handed arrangement (Table 1 and Supplementary Figure 3).

In addition to successfully assigning each couplet to its naphthalene chromophore, the hypochromic decrease of the naphthalene groups is revealed by deriving the absorbance changes over the course of self-assembly (Supplementary Figure 5). These phenomena are consistent with the increasing proximity and stacking of the naphthalene groups over time and congruous with the observed induced naphthalene chirality. We note that changes in chirality have been observed elsewhere for related Fmoc-amino acid and Fmoc-dipeptide based gelators [27-30] where the chirality changes could be correlated to specific functional groups on one of the amino acids, not to a specific amino acid sequence. Previously, changes in the chirality for the self-assembled structures for naphthalene-dipeptides has been driven by changes in the chirality of the amino acids.[36] However, here we find that dipeptide sequence is critical and the helicity can be inverted even with L-amino acids. The helicity determination of the dipeptide sequence also dominates over specific electron-withdrawing or –donating groups on the naphthalene ring. These conclusions are drawn from the results of our examination of the library studied here. Further dipeptides may differ in the rules that govern the helicity. Nonetheless, the data clearly shows that a change in dipeptide sequence can directly impact on the helicity of the fibre, despite both amino acids being of the same chirality.

System	Helicity	Origin / nm
H-Nap-AA	R	220 – nap
H-Nap-AV	L	224 – nap
Br-Nap-AA	R	226 – nap
Br-Nap-AV	L	223 – nap
CN-Nap-AA	-	-
CN-Nap-AV	L	229 – nap

Table 1. The exciton couplets exhibited by the dipeptides as observed by deconvoluted circular dichroism indicating the helicity of the systems and the origins of these (see Supplementary Figure 3). The chirality of CN-Nap-AA has not been assigned due to poor fitting.

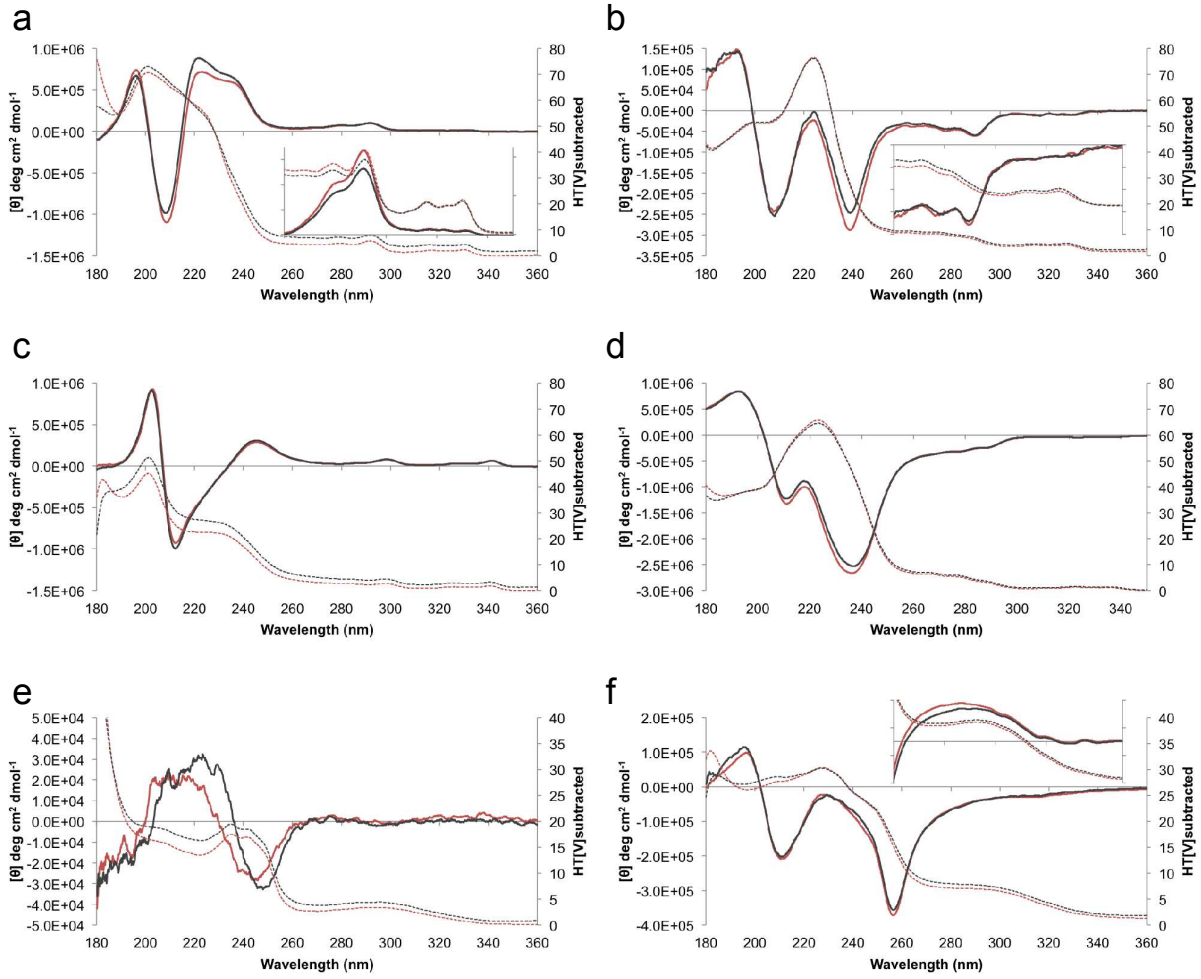

Figure 3. Circular dichroism spectra of the naphthalene aliphatic dipeptides (5mg mL^{-1}) (black traces) (a) H-Nap-AA, (b) H-Nap-AV, (c) Br-Nap-AA, (d) Br-Nap-AV, (e) CN-Nap-AA and (f) CN-Nap-AV. Significant LD artefacts are not present as indicated by the overlay of the 0° and 90° cuvette rotations (black and red traces respectively). Dotted lines show the buffer subtracted HT trace, equivalent to the dipeptide absorbance, revealing the naphthalene absorbance maxima. Inserts show expanded spectra for the near UV (250–360 nm).

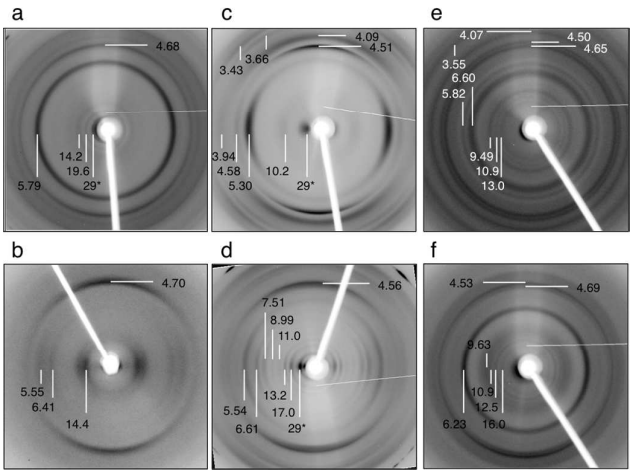

Figure 4. fXRD from aligned fibrils of the aliphatic di-peptides (a) H-Nap-AA, (b) H-Nap-AV, (c) Br-Nap-AA, (d) Br-Nap-AV, (e) CN-Nap-AA and (f) CN-Nap-AV. The pattern shown for H-Nap-AA has been previously published,[37] but is included here for comparison. All fibre axes are vertical. *Reflections partially occluded by the backstop were measured manually.

Molecular packing is governed by the naphthalene moiety

fXRD patterns were collected from aligned samples of the hydrogels, prepared by air-drying the gels to form an aligned fibre sample. To ensure that the architecture of self-assembled fibres is the same in the hydrated and dried state, fXRD patterns were compared from aligned samples in the hydrated, semi-hydrated and air-dried state by collecting data as the hydrogel droplet dried. All patterns, with the exception of H-Nap-AA and CN-Nap-AA (Figure 4e), exhibit high levels of directionality indicating successful alignment and permitting the assignment of repetitive interatomic distances to discrete molecular axes. We note from TEM that the fibrils of H-Nap-AA and CN-Nap-AA in solution are thinner than the others systems (Figure 2) indicating lower degrees of lateral association and perhaps resulting in poorer reinforcement of aligned signals. The observed diffraction signal positions and axial alignments were the same throughout each hydration state, supporting the view that the architecture is the same in solution as in the aligned state (Figure 4 and Supplementary Figure 6). Samples with similar levels of alignment were compared to enable comparison between major meridional and equatorial reflection position and relative intensities (Figure 4). Diffraction signals on the meridian and equator align to the long axis of the fibril and lateral axis respectively, whereby meridionals report on interstrand distances, whilst equatorials arise from lateral packing and intersheet distances. The patterns all indicate a short-range repetitive spacing along the fibre axis of 4.51 – 4.75 Å, consistent with the expected distance between hydrogen-bonded ß-strands.[38, 39] Similar values have been found elsewhere for Fmoc-dipeptides, and have been ascribed to either distances between ß-sheets or distances between the Fmoc groups. [32, 40-42] The interstrand separation in Å, indicated by the strongest meridional signals, are generally grouped by the identity of the naphthalene group since H-Nap-AA and H-Nap-AV show a meridional repeat of 4.68 – 4.70 Å whilst the peptides containing Br or CN have shorter repeats closer to 4.55 Å (Table S3). Reflection positions, relative intensity and axial alignment of reflections for each fXRD pattern must arise from the molecular packing of the dipeptides in the self-assembled fibres. The variable equatorial diffraction signals for each system reflect the differences in lateral packing of the assemblies, consistent with observations of variable lateral packing morphologies in the TEM (Figure 2). Comparison of the reflection positions reveals a close similarity of the equatorial signals between systems with the same naphthalene conjugate i.e. Br-Nap, CN-Nap or H-Nap (Supplementary Table 3). Br-Nap-AA and Br-Nap-AV patterns share a very clear long-range equatorial reflection at 29 Å, which could correlate with a protofilament diameter (although we note that the TEM shows the fibres have significantly higher diameters, presumably due to lateral association of the protofilaments). Reflections at approximately 26 Å have been found for Fmoc-dipeptides and ascribed to the fibre widths.[32, 40, 42] This data has been used to build a model for the assembly, although it is not clear to us that this model can be directly translated to our systems. Further, the reflections with the greatest relative intensity are matched in Br-Nap and CN-Nap systems. These intense reflections may arise from the dominant interatomic separations adopted by these self-assemblies. We postulate that the lateral molecular packing of the dipeptide self-assemblies is governed by the geometric, steric and possibly electrostatic constraints imposed by the naphthalene group in each system, although we acknowledge this suggestion arises from a small subset of all possible naphthalene-dipeptide gelators.

Conclusions

The library of dipeptides explored here, all self-assemble via a pH switch, into fibrils of indeterminate length with a varying morphological and cross-linked appearance. Different features of the molecular architectures underlying these anisotropic assemblies is determined independently by the nature of the naphthalene conjugate and by the amino acid sequence (summarised in Table 2). Chiral naphthalene ordered assemblies are observed to form and have a helicity that implies they may form a core of the fibrils. The handedness of the naphthalene helicity is governed by the peptidic content of the dipeptide, where Ala-Ala and Ala-Val leads to right and left handed helices respectively. Helical characteristics are implied by the CD data whilst a crystalline lattice is probed by fXRD. Electron microscopy and fXRD reveal that the packing of these lattices must occur over dimensions much larger than the dipeptides themselves and therefore arises from the regular packing of filaments as well as the local molecular architecture. fXRD reveals that the assemblies exhibit short-range packing interactions reminiscent of amyloid self-assembly with interatomic separation along the fibre axis on the order of 4.5 – 4.7 Å, consistent with hydrogen bonding of ß-strands.

System	Fibril morphology	Chirality	Orientation	Meridional Major	Equatorial Major	Equatorial Long range
H-Nap-AA (a)	Very thin filaments (~7 nm)	R	Poor	4.68 Å	5.79Å	14.2 Å & 19.6 Å ~29 Å
H-Nap-AV (b)	Thick /twisted filaments (variable widths)	L	Aligned	4.70 Å	5.55 Å or 6.41 Å	14.40 Å -
Br-Nap-AA (c)	Crystalline nanotube of individual protofilaments (~20 nm)	R	Aligned	4.51 Å	5.30 Å	10.2 Å ~29 Å
Br-Nap-AV (d)	Thick filaments/tubes (variable widths)	L	Aligned	4.56 Å	5.54 Å	13.2 Å & 17 Å ~29 Å
CN-Nap-AA (e)	Very thin filaments (14-15 nm)	--	Poor	4.65 and 4.5 Å	6.60 Å	9.49 Å & 13.0 Å
CN-Nap-AV (f)	Twisted filaments (14-15 nm)	L	Aligned	4.56 Å	6.23 Å	10.9 Å & 16.0 Å

Table 2. A summary of the material, structural and morphological characteristics of each dipeptide system of the library.

In contrast to the dipeptide sequence governing the assemblies helicity, the precise hydrogen bonded separation is governed by the nature of the naphthalene conjugate, whilst also the naphthalene conjugate is found to determine the major interatomic separations of the lateral molecular packing.

Whilst both the naphthalene and inter-ß-strand interactions are presumably essential for the formation of the structures observed we cannot deduce which interaction, if any, principally drives self-assembly into the specific aggregates. For related Fmoc-dipeptide systems, it has been suggested that the driving force is assembly of the aromatic rings.[32, 40-42] Related work on a system where one amino acid was replaced with lactic acid showed that the formation of beta-sheets is not a pre-requisite for gelation (and also makes the point that interpretation of IR data is difficult for such short peptides).[40] In general, dipeptides such as those described here form micellar aggregates at high pH (i.e. before gelation), presumably associating via hydrophobic interactions lead by the aromatic rings.[43, 44] Nonetheless, whilst the naphthalene rings are undoubtedly essential for self-assembly, which interactions lead to the assembly into anisotropic fibres and modulate the nature of the final assembled structure is less clear. A key issue in the area of low molecular weight gelators is the lack of available design rules for their design. [45] This work points to important contributions of different parts of the molecule to the organisation of both molecular structure within individual filaments and their lateral association and packing. However, we note that it is not possible to link the molecular structure to the bulk properties of the gels. This is unsurprising, since it is increasingly clear that the mechanical properties of the final gels are driven not only by the primary self-assembled structures, but also by aspects such as entanglements and the number of cross-links, which are influenced by the process and kinetics of assembly and not measured at the length scales investigated here.

Experimental

Di-peptide synthesis

All dipeptides were synthesised as described previously. Full characterisation details can be found elsewhere.[26]

Di-peptide gelation

All dipeptides were dissolved in milliQ H_2O at a concentration of 5 $mgmL^{-1}$ and pH 10.5. Gelation was initiated by dissolution of GdL at 8.9 $mgmL^{-1}$ by gentle but thorough mixing. In all cases gelation was initiated at room temperature. Final pH is 4.6.

Transmission electron microscopy

To sample the hydrogel material for TEM, grids (Agar Scientific, Carbon/Formvar Cu Mesh) were incubated on gelling drops of dipeptide solution in a humid atmosphere to prevent dehydration. Grids were removed and stained with 2% w/v uranyl acetate for visualisation on a Hitachi 7100 TEM with an axially mounted Gatan camera for digital image acquisition. CN-Nap-AV was found to not adhere to the grid surface and so 1 µL was gelled and subsequently dried to the grid surface to enable visualisation of the sample.

Circular dichroism

Circular dichroism spectra were collected using a Jasco J-715 spectropolarimeter equipped with a Peltier temperature controller. Spectra were collected at 21 °C, between 500 – 180 nm with a resolution of 0.1 nm and bandwidth of 1 nm. Three scans were accumulated, averaged and processed by subtracting a GdL spectrum. Spectra were collected overnight on samples in 0.01 mm demountable quartz

cuvettes (Hellma) to minimise the HT[V] below 600. The measured high tension voltage (HT[V]) was subsequently processed by subtracting HT[V] from solvent and GdL to account for the light scattering from the solvent and GdL revealing the absorbance spectrum of the sample. Spectra were collected at 0° and 90° degree cuvette rotations to ensure no effects from sample anisotropy lead to linear dichroic artefacts. Samples were gelled in cuvettes overnight to avoid sampling issues from pre-formed gels. This also ensured complete self-assembly and permitted the accurate subtraction of the spectra arising from the GdL background. Circular dichroism spectra were deconvoluted using least squares fitting performed in Excel utilising Solver (GRG Nonlinear Engine). Exciton couplets were modelled as Gaussian curves with equal peak widths and absolute magnitudes.

FTIR

IR spectra were collected on a Bruker Tensor 27 FTIR spectrometer at a resolution of 2 cm–1 with spectral averaging over 64 scans. All hydrogels were prepared in D2O using NaOD (0.1 M) to change the pD. The hydrogels were loaded onto a CaF2 window, and another CaF2 window was used to sandwich the gels. Each FTIR spectrum was background corrected by subtraction of a D2O spectrum. For all spectra, the peaks exhibited in the region between 1500 and 1800 cm–1 are shown in the Supplementary Table 1.

X-ray fibre diffraction

10 μL of gelating solution was suspended between two wax tipped capillary tubes immediately after GdL dissolution and allowed to air dry to produce a partially aligned fibre bundle on one capillary. Fibres of H-Nap-AV were only found to align after allowing 2 hours of gelation before alignment. The fibre sample was mounted on a goniometer head and X-ray diffraction data were collected using a Rigaku rotating anode (CuK□) source with VariMax-HF mirrors and Saturn 944+ CCD detector. Exposure times were between 10 and 30 s. The data were examined using Imosflm [46] and Clearer was used to make measurements of diffraction signal positions [47].

Hydrated fibre X-ray diffraction

10 μL of gelating solution (5 mgmL-1) was suspended between two wax capillaries immediately after GdL dissolution in a dehydration cell similar to devices reported elsewhere [48] and as previously reported [25]. Diffraction data were collected at the point of fibril alignment whilst still in the hydrated state. Data were collected using a Rigaku 007HF Cu Kα (λ 1.5419 Å) rotating anode generator with VariMax-HF mirrors and Saturn 944+ CCD detector. Exposure times were 30 seconds and corrected specimen to detector distances 51.2mm. The detector recorded images at 1042 x 1042 px in (2×2 binning mode). Contrast ratio was maintained across the time course to allow the accurate comparison of the relative intensities of diffraction signals. Data was opened with mosflm and processed using CLEARER.

Acknowledgements

DA and LC acknowledge funding from EPSRC (EP/G012741/1). We thank Julian Thorpe for valuable help with TEM.

Notes

[a] 1 School of Life Sciences, University of Sussex, Falmer, Brighton, BN1 9QG, United Kingdom, L.C.Serpell@sussex.ac.uk
[b] Department of Chemistry, University of Warwick, Coventry, CV4 7AL, United Kingdom
[c] Department of Chemistry, University of Liverpool, Crown Street, Liverpool, L69 7ZD, United Kingdom
*To whom correspondence should be addressed

Electronic Supplementary Information (ESI) available: [Tables showing exciton couplets positions for CD data, diffraction signal positions from fXRD and FTIR peak positions. Figures showing development of CD spectra with time, deconvoluted spectra, absorbance spectra and hydrated fXRD patterns]. See DOI: 10.1039/b000000x/

References

1. J. W. Steed, *Chem. Commun.*, 2011, **47**, 1379-1383.
2. P. Terech and R. G. Weiss, *Chem. Rev.*, 1997, **97**, 3133-3159.
3. B. Xu, Z. M. Yang, G. L. Liang, M. L. Ma and Y. Gao, *J. Mater. Chem.*, 2007, **17**, 850-854.
4. D. J. Adams, L. M. Mullen, M. Berta, L. Chen and W. J. Frith, *Soft Matter*, 2010, **6**, 1971-1980.
5. M. Hughes, P. W. J. M. Frederix, J. Raeburn, L. S. Birchall, J. Sadownik, F. C. Coomer, I. H. Lin, E. J. Cussen, N. T. Hunt, T. Tuttle, S. J. Webb, D. J. Adams and R. V. Ulijn, *Soft Matter*, 2012, **8**, 5595-5602.
6. D. J. Adams, *Macromol. Biosci.*, 2011, **11**, 160-173.
7. C. Tomasini and N. Castellucci, *Chem. Soc. Rev.*, 2013, **42**, 156-172.
8. J. Raeburn, A. Zamith Cardoso and D. J. Adams, *Chem. Soc. Rev.*, 2013, **42**, 5143-5156.
9. A. Mahler, M. Reches, M. Rechter, S. Cohen and E. Gazit, *Adv. Mater.*, 2006, **18**, 1365-1370.
10. V. Jayawarna, M. Ali, T. A. Jowitt, A. E. Miller, A. Saiani, J. E. Gough and R. V. Ulijn, *Adv. Mater.*, 2006, **18**, 611-614.
11. Y. Zhang, Z. M. Yang, F. Yuan, H. W. Gu, P. Gao and B. Xu, *J. Am. Chem. Soc.*, 2004, **126**, 15028-15029.
12. Z. J. Qiu, H. T. Yu, J. B. Li, Y. Wang and Y. Zhang, *Chem. Commun.*, 2009, 3342-3344.
13. D. J. Adams, M. F. Butler, W. J. Frith, M. Kirkland, L. Mullen and P. Sanderson, *Soft Matter*, 2009, **5**, 1856-1862.
14. Z. Yang, H. Gu, D. Fu, P. Gao, J. K. Lam and B. Xu, *Adv. Mater.*, 2004, **16**, 1440-1444.
15. R. Vegners, I. Shestakova, I. Kalvinsh, R. M. Ezzell and P. A. Janmey, *Journal of peptide science : an official publication of the European Peptide Society*, 1995, **1**, 371-378.
16. R. V. Rughani, D. A. Salick, M. S. Lamm, T. Yucel, D. J. Pochan and J. P. Schneider, *Biomacromolecules*, 2009, **10**, 1295-1304.

17. A. Dasgupta, J. H. Mondal and D. Das, *RSC Advances*, 2013, **3**, 9117-9149.
18. D. J. Adams, K. Morris, L. Chen, L. C. Serpell, J. Bacsa and G. M. Day, *Soft Matter*, 2010, **6**, 4144-4156.
19. N. Javid, S. Roy, M. Zelzer, Z. Yang, J. Sefcik and R. V. Ulijn, *Biomacromolecules*, 2013, **14**, 4368-4376.
20. L. Chen, K. Morris, A. Laybourn, D. Elias, M. R. Hicks, A. Rodger, L. Serpell and D. J. Adams, *Langmuir*, 2010, **26**, 5232-5242.
21. M. Hughes, L. S. Birchall, K. Zuberi, L. A. Aitken, S. Debnath, N. Javid and R. V. Ulijn, *Soft Matter*, 2012, **8**, 11565-11574.
22. A. M. Smith, R. J. Williams, C. Tang, P. Coppo, R. F. Collins, M. L. Turner, A. Saiani and R. V. Ulijn, *Adv. Mater.*, 2008, **20**, 37-41.
23. S. Fleming and R. V. Ulijn, *Chem. Soc. Rev.*, 2014.
24. M. Reches and E. Gazit, *Nature Nanotechnology*, 2006, **1**, 195-200.
25. K. A. Houton, K. L. Morris, L. Chen, M. Schmidtmann, J. T. A. Jones, L. C. Serpell, G. O. Lloyd and D. J. Adams, *Langmuir : the ACS journal of surfaces and colloids*, 2012, **28**, 9797-9806.
26. L. Chen, S. Revel, K. Morris, L. C. Serpell and D. J. Adams, *Langmuir*, 2010, **26**, 13466-13471.
27. D. M. Ryan, T. M. Doran, S. B. Anderson and B. L. Nilsson, *Langmuir*, 2011, **27**, 4029-4039.
28. D. M. Ryan, S. B. Anderson and B. L. Nilsson, *Soft Matter*, 2010, **6**, 3220-3231.
29. M. Reches and E. Gazit, *Physical Biology*, 2006, **3**, S10-S19.
30. C. G. Pappas, Y. M. Abul-Haija, A. Flack, P. W. J. M. Frederix and R. V. Ulijn, *Chem. Commun.*, 2014, **50**, 10630-10633.
31. J. T. Pelton and L. R. McLean, *Anal. Biochem.*, 2000, **277**, 167-176.
32. X. Mu, K. M. Eckes, M. M. Nguyen, L. J. Suggs and P. Ren, *Biomacromolecules*, 2012, **13**, 3562-3571.
33. K. E. Marshall, M. R. Hicks, T. L. Williams, S. V. Hoffmann, A. Rodger, T. R. Dafforn and L. C. Serpell, *Biophys. J.*, 2010, **98**, 330-338.
34. K. L. Morris, A. Rodger, M. R. Hicks, M. Debulpaep, J. Schymkowitz, F. Rousseau and L. C. Serpell, *Biochem. J*, 2013, **450**, 275-283.
35. J. Rajendra, M. Baxendale, L. G. D. Rap and A. Rodger, *J. Am. Chem. Soc.*, 2004, **126**, 11182-11188.
36. Z. Yang, G. Liang, M. Ma, Y. Gao and B. Xu, *J. Mater. Chem.*, 2007, **17**, 850-854.
37. K. L. Morris, L. Chen, J. Raeburn, O. R. Sellick, P. Cotanda, A. Paul, P. C. Griffiths, S. M. King, R. K. O'Reilly, L. C. Serpell and D. J. Adams, *Nat Commun*, 2013, **4**, 1480.
38. A. J. Geddes, K. D. Parker, E. D. Atkins and E. Beighton, *J. Mol. Biol.*, 1968, **32**, 343-358.
39. L. Pauling and R. B. Corey, *Proceedings of the Royal Society of London Series B-Biological Sciences*, 1953, **141**, 21-33.
40. K. M. Eckes, X. Mu, M. A. Ruehle, P. Ren and L. J. Suggs, *Langmuir : the ACS journal of surfaces and colloids*, 2014, **30**, 5287-5296.
41. C. Tang, R. V. Ulijn and A. Saiani, *The European physical journal. E, Soft matter*, 2013, **36**, 111.
42. A. M. Smith, R. J. Williams, C. Tang, P. Coppo, R. F. Collins, M. L. Turner, A. Saiani and R. V. Ulijn, *Advanced materials*, 2008, **20**, 31-41.
43. L. Chen, G. Pont, K. Morris, G. Lotze, A. Squires, L. C. Serpell and D. J. Adams, *Chemical communications*, 2011, **47**, 12071-12073.
44. L. Chen, T. O. McDonald and D. J. Adams, *RSC Advances*, 2013, **3**, 8714-8720.
45. R. G. Weiss, *J Am Chem Soc*, 2014, **136**, 7519-7530.
46. A. G. W. Leslie, *Recent changes to the MOSFLM package for processing film and image plate data*, 1992.
47. O. S. Makin, P. Sikorski and L. C. Serpell, *J. Appl. Crystallogr.*, 2007, **40**, 966-972.
48. M. McDonald, A. Kendalla, M. Tanaka, J. S. Weissman and G. Stubbs, *J. Appl. Crystallogr.*, 2008, **41**, 206-209.

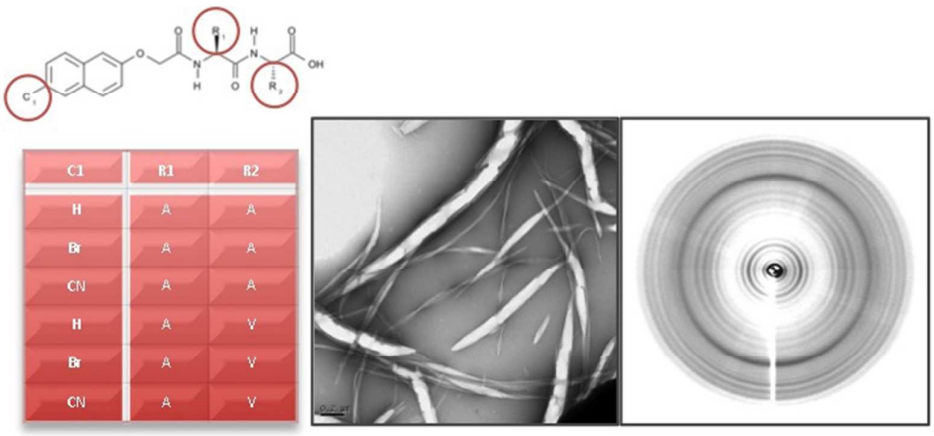

The structures of hydrogels formed by naphthalene dipeptide library were explored using a combined approach of electron microscopy, Xray fibre diffraction and circular dichroism
254x142mm (72 x 72 DPI)

Structural determinants in a library of low molecular weight gelators

Kyle L. Morris,[a,b] Lin Chen,[c] Alison Rodger,[b] Dave J. Adams[c] and Louise C. Serpell[a*]

Supplementary Information

The supplementary data tabulates the spectroscopic biophysical and structural data collected on gelated dipeptides from FTIR (Table S1), CD (Table S2) and fXRD (Table S3). Table S2 tabulates the Gaussian peak fitting for the CD spectra and compares the couplet x-intercept (mid-point – theoretical absorbance maxima for fitted couplet) to the experimentally measured absorbance maxima.

The CD spectra for the gelating dipeptides increase in intensity over the time course of gelation as shown in Figure S1. Absolute signal intensities were found to vary between experiments on the same system, although the sign of the peaks was found to be reproducible. This may be attributable to varying amounts of helical species (left or right) affecting the intensities of the exciton-dominated spectra. Nevertheless, the consistent sign of the peaks indicates reproducible dominance of the helical species described in the `main text. The spectra of 2-Nap AV was found to arise only after overnight incubation and CN-Nap AA did not develop any signal detectable above that of GdL. An additional couplet was observed for CN-Nap-AV with negative and positive peaks at 243 and 226 nm respectively. This couplet was not observed after overnight incubation but is used in subsequent deconvolutions. Gaussian fitting of the transitions giving rise to the CD spectra are deconvoluted and shown in Figure S2. The sign of the fitted peaks around the naphthalene absorbance maxima previously identified was used to assign naphthalene chiral assembly handedness. A long wavelength negative to short wavelength positive component indicates a left-handed and vice versa for right-handed assemblies.[1]

The indication of the close association of naphthalene groups into chiral assemblies is further indicated by the hypochromic shifting of the naphthalene absorbance maxima. Absorbance maxima may be derived from HT[V] data collected by CD measurements as shown in Figure S3. The net hypochromic shifting of naphthalene absorbance maxima is then revealed over the course of self-assembly and gelation in Figure S4.

The spectroscopic data was collected in the hydrated state whereas the structural fXRD data collected in the dried state. Figure S5 demonstrates that the diffraction signals arising from the dipeptide structure are preserved in the hydrated state. Each system exhibits strong diffraction from water at ~3 Å and the reflections arising from the structure of the dipeptide are identical to those in the dried state (see Figure 4) indicating the structure of the self-assemblies is the same in the hydrated and dried state.

Table S1. The FTIR peaks exhibited by each system in the self-assembled gel phase between 1700 – 1600 cm^{-1}. *Indicates broad overlapping peaks

System	Peak 1 / cm^{-1}	Peak 2 / cm^{-1}	Peak 3 / cm^{-1}	Peak 4 / cm^{-1}
H-Nap-AA	1712	1644	1629	1666*
H-Nap-AV	1724	1651	1629	
Br-Nap-AA	1735	1652	1633	
Br-Nap-AV	1721	1645	1628	1680*
CN-Nap-AA	1713		1627	1664
CN-Nap-AV	1734	1648	1626	

Table S2. Exciton couplets established from spectra deconvolution

System	High-energy couplet (nm)	Sign	Low-energy couplet (nm)	Sign	Helicity	Couplet mid-point (nm)	Absorbance peak (nm)
H-Nap-AA	212.4	-	218.8	+	R	215.6	220.2
H-Nap-AA	197.5	+	205.8	-	L	201.7	201.1
H-Nap-AV	219.4	+	238.8	-	L	229.1	224.0
H-Nap-AV	196.2	+	206.0	-	L	201.1	200.7
Br-Nap-AA	222.6	-	246.2	+	R	234.4	226.0
Br-Nap-AA	206.5	+	208.3	-	L	207.4	201.0
Br-Nap-AV	218.7	+	238.4	-	L	228.5	223.3
Br-Nap-AV	199.1	+	213.3	-	L	206.2	~190
CN-Nap-AA	-		-		-	-	-
CN-Nap-AA	-		-		-	-	-
CN-Nap-AV	234.3	+	236.9	-	L	235.6	229.1
CN-Nap-AV	199.9	+	207.4	-	L	203.6	~207

Table S3. The position, axial alignment and relative intensity of the equatorial and meridional reflections pertaining to the structure of the aliphatic di-peptides. The axial alignment of the reflections exhibited by CN-AA are concluded from comparison to other patterns and relative signal positions.

***Reflections near the backstop and thus partially occluded were measured manually, in these cases relative intensity was not measured. [+]Where reflection axis is not apparent due to radial averaging assignment was made by comparison to reflections from other patterns.**

H-Nap-AA

Peak resolution (Å)	Relative intensity	Axis
29	*	E
19.61	0.58	E
14.16	**0.61**	**E**
-	-	-
5.79	**1.00**	**E**
4.68	**0.80**	**M**

H-Nap-AV

Peak resolution (Å)	Relative intensity	Axis
-	-	-
-	-	-
14.37	**0.97**	**E**
6.41	0.73	E
5.55	**0.73**	**E**
4.70	**1.00**	**M**

Br-Nap-AA

Peak resolution (Å)	Relative intensity	Axis
29	*	E
-	-	-
-	-	-
10.23	0.48	E
-	-	-
-	-	-
-	-	-
5.30	**1.00**	**E**
-	-	-
4.58	0.62	E
3.94	0.63	E
-	-	-
4.51	**0.99**	**M**
-	-	-
4.09	0.92	M
3.66	0.64	M
3.43	0.60	M

Br-Nap-AV

Peak resolution (Å)	Relative intensity	Axis
29	*	E
16.95	0.66	E
13.20	0.58	E
10.95	0.50	E
8.99	0.51	E
7.51	0.61	E
6.61	0.69	E
5.54	**0.83**	**E**
-	-	-
-	-	-
-	-	-
-	-	-
4.56	**1.00**	**M**
-	-	-
-	-	-
3.79	0.80	OM
-	-	-

CN-Nap-AA

Peak resolution (Å)	Relative intensity	Axis
-	-	-
12.96	0.76	E^+
10.93	0.77	E^+
9.49	0.83	E^+
6.60	**0.95**	**E^+**
5.82	0.87	-
4.65	**1.00**	**M^+**
4.50	0.85	M^+
4.07	0.94	-
3.55	0.89	-

CN-Nap-AV

Peak resolution (Å)	Relative intensity	Axis
15.97	0.66	E
12.46	0.69	E
10.86	*	E
9.63	0.74	E
6.23	**0.97**	**E**
-	-	-
4.69	*****	**M**
4.53	1.00	M
-	-	-
-	-	-

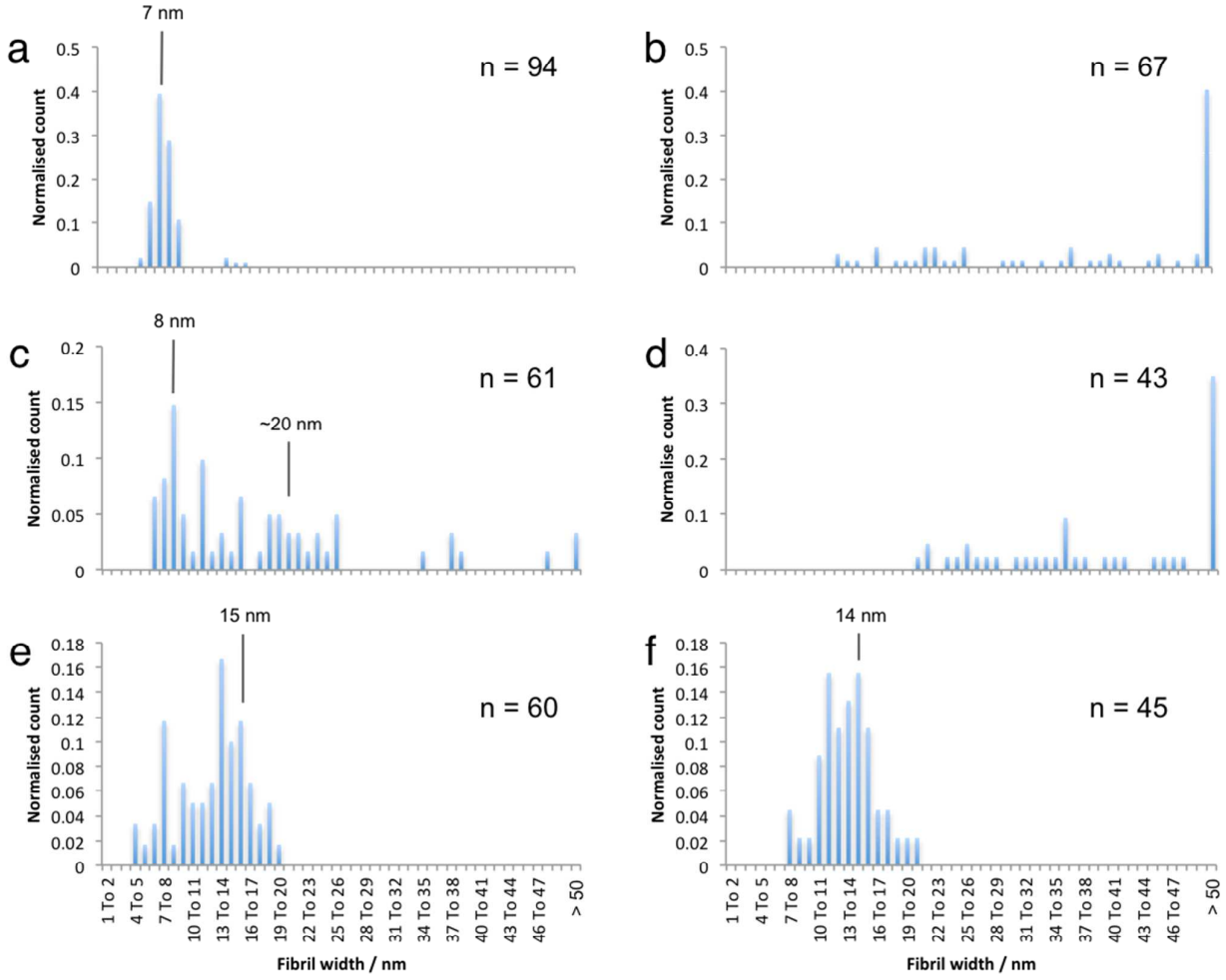

Figure S1. Analysis of fibril morphology by characterisation of fibril width. (a) H-Nap-AA, (b) H-Nap-AV, (c) Br-Nap-AA, (d) Br-Nap-AV, (e) CN-Nap-AA and (f) CN-Nap-AV. Unbiased measurements were made on the micrographs (Figure 2) and the distribution of sizes plotted by histogram, sizes corresponding to predominantly observed fibril widths are highlighted.

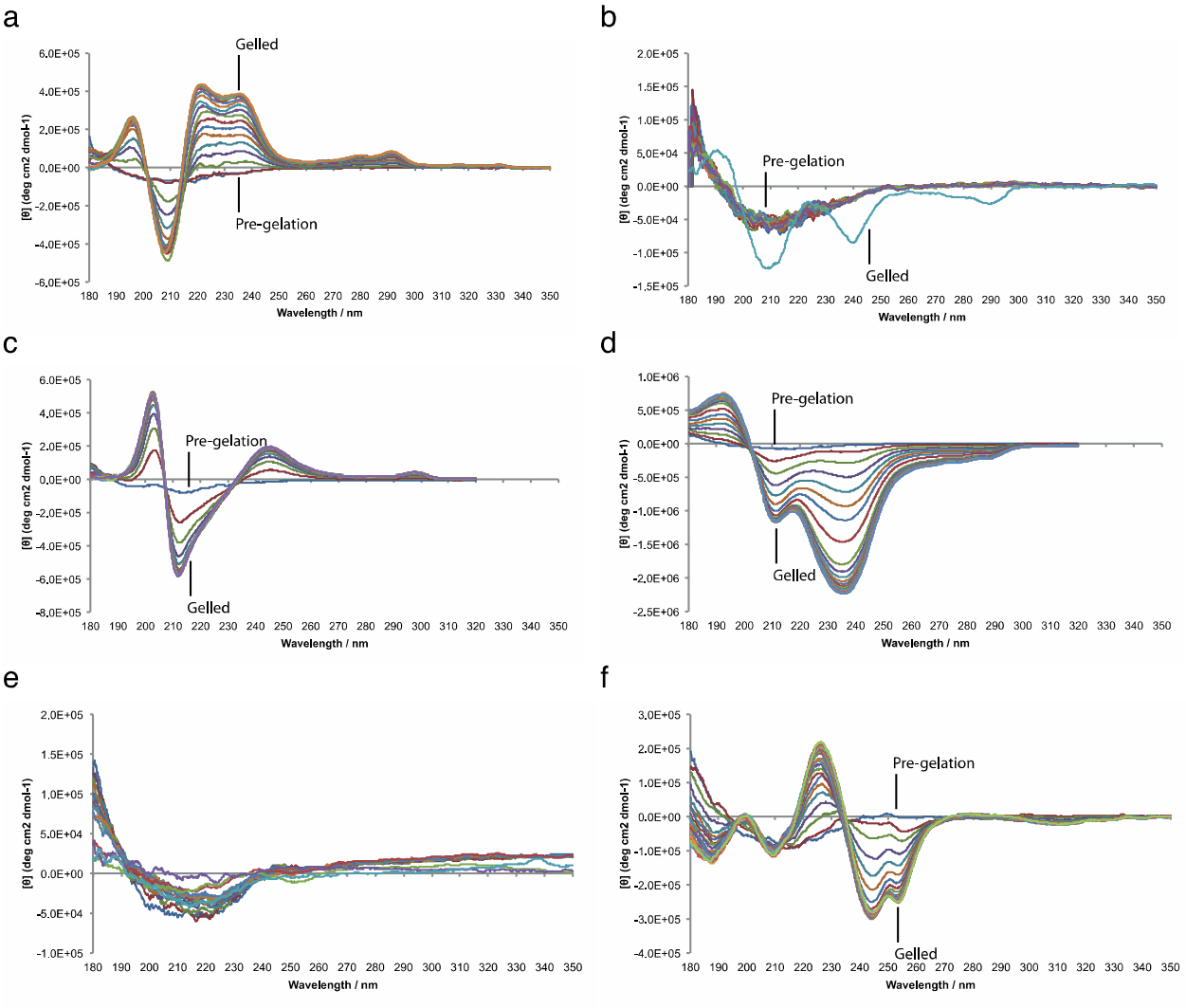

Figure S2. The development of circular dichroism signals over the course of *in situ* self-assembly and gelation. All signals increase from the background spectra to the characteristic peak profiles shown in the main text (Figure 3). (a) H-Nap-AA, (b) H-Nap-AV, (c) Br-Nap-AA, (d) Br-Nap-AV, (e) CN-Nap-AA, (f) CN-Nap-AV. Data collected on a Jasco J-715 spectropolarimeter at 21 °C in a 0.01 mm pathlength.

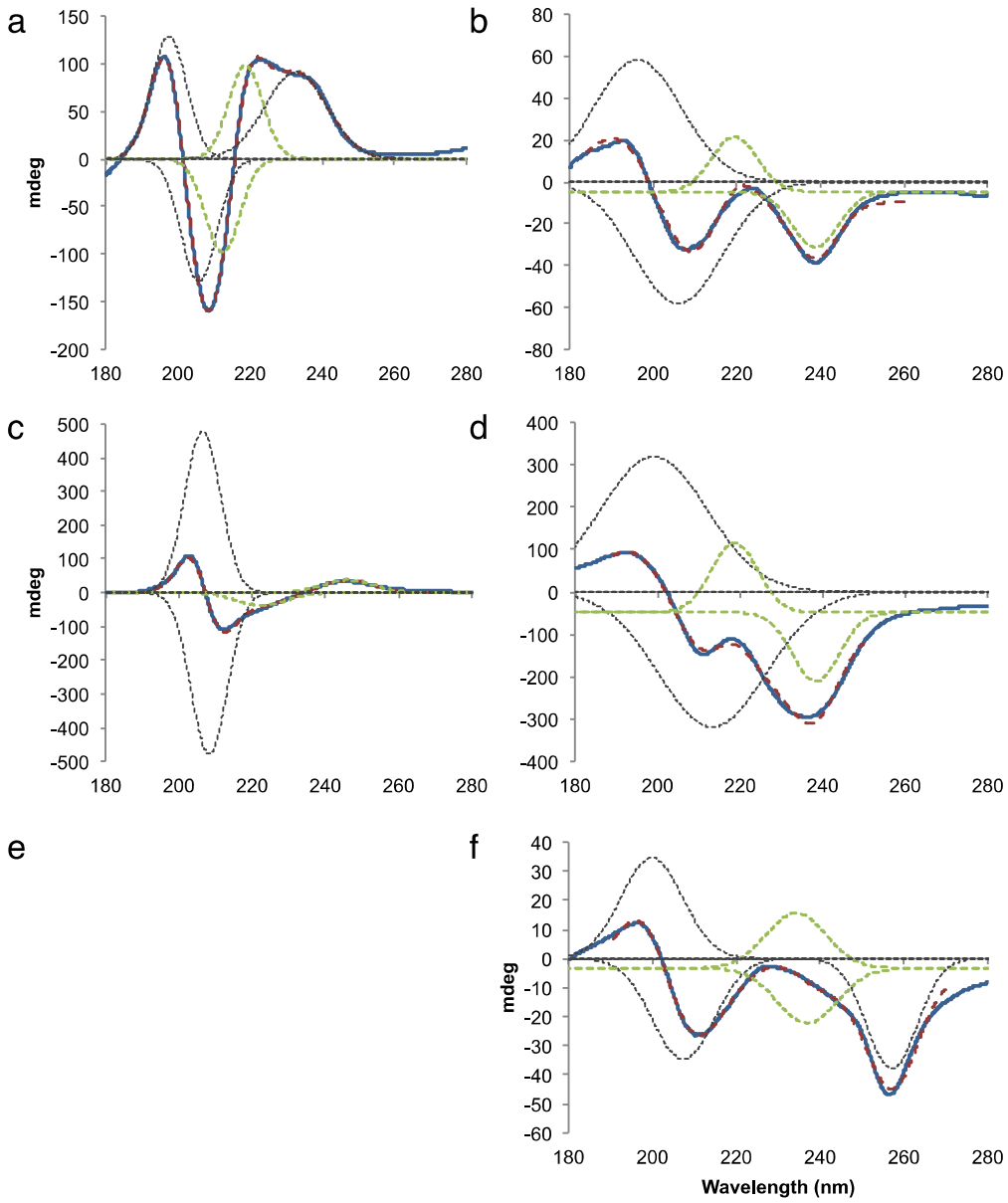

Figure S3. Spectra of Figure S1 collected at completion of gelation and deconvolved to reveal the Gaussian components of each CD spectra. The (blue solid) experimental data, (dashed red) fitted data, (grey dashed) fitted Gaussian components and (green dashed) exciton couplets modeled to arise from interactions of the naphthalene groups are shown. Minimised sum of square fitting was performed between approximately 190 – 260 nm. (a) H-Nap-AA, (b) H-Nap-AV, (c) Br-Nap-AA, (d) Br-Nap-AV, (e) Data deconvolution not possible, (f) CN-Nap-AV.

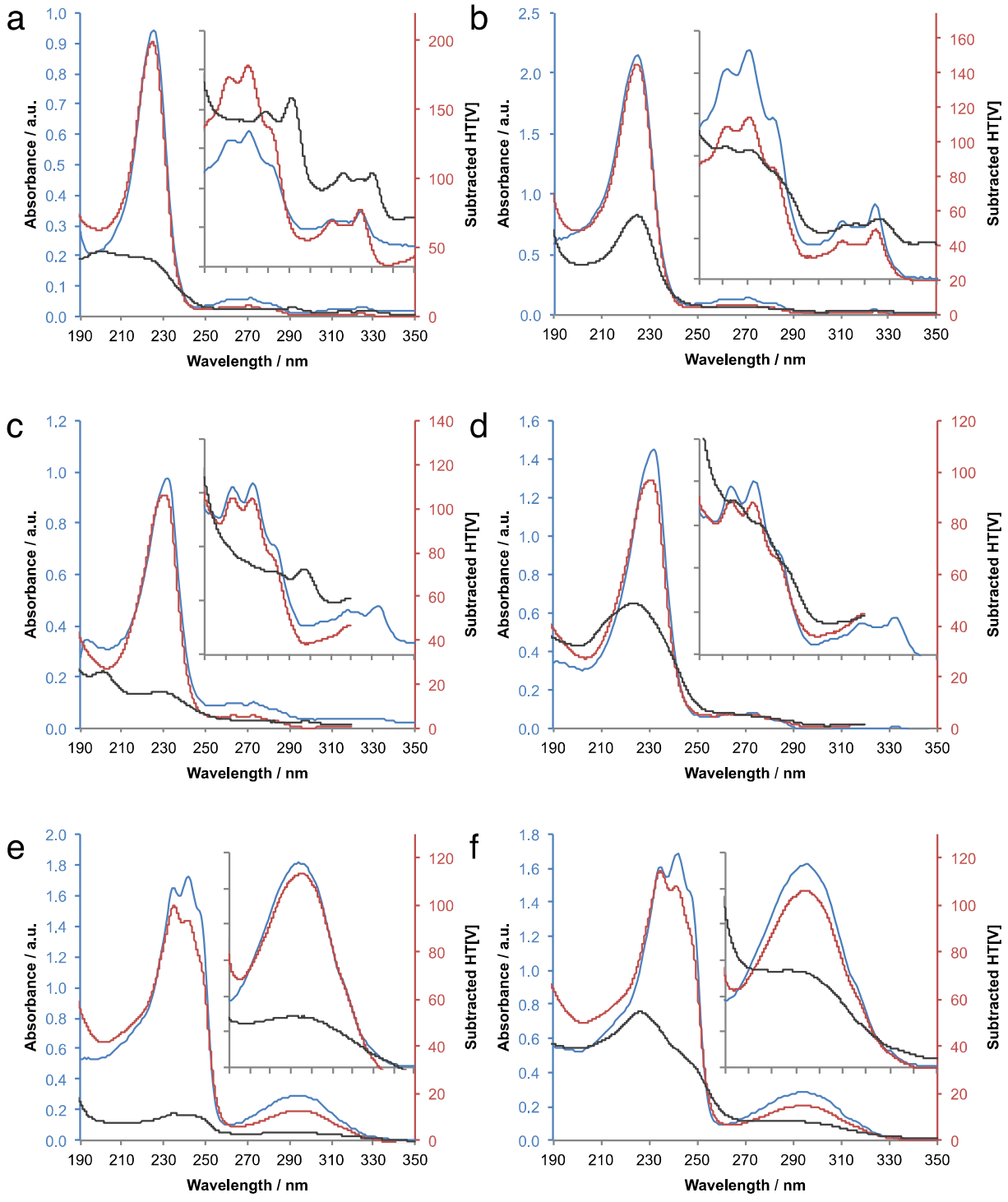

Figure S4. Absorption data for the dipeptide systems including (blue) UV/Vis absorbance and (red) HT[V] of stock before gelation compared to (black) HT[V] exhibited by gelled solutions. HT[V] values have been buffer subtracted to reveal the absorbance spectrum from the sample. The overlay of the UV/Vis and HT[V] data demonstrates the validity of subtracted HT[V] data as an absorbance measurement. UV/Vis data collected on a Shimadzu UV/Vis UV2400PC in a 1 cm pathlength at room temperature. HT[V] data collected on a Jasco J-715 spectropolarimeter at 21 °C in a 0.01 mm pathlength. (a) H-Nap-AA, (b) H-Nap-AV, (c) Br-Nap-AA, (d) Br-Nap-AV, (e) CN-Nap-AA, (f) CN-Nap-AV

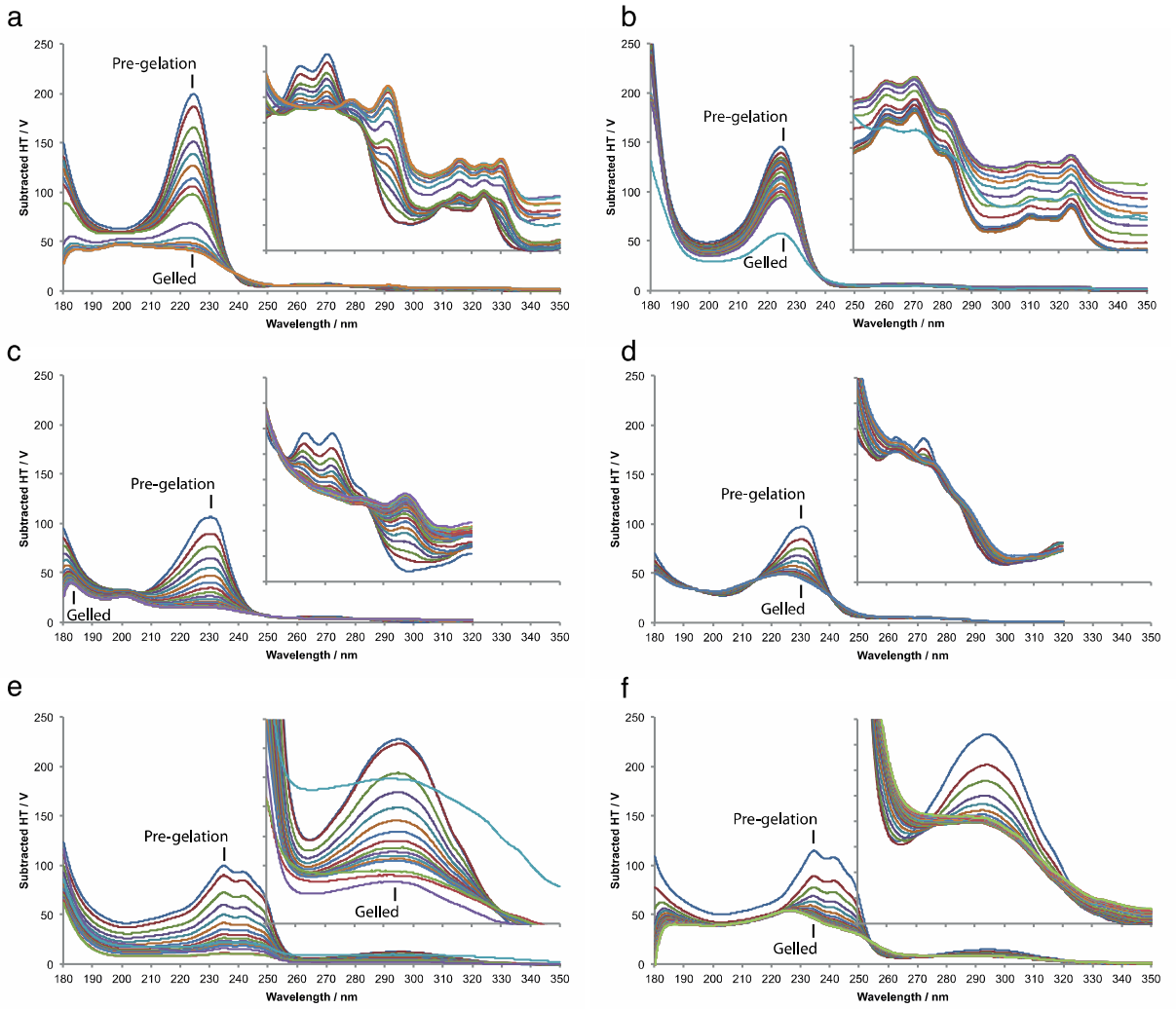

Figure S5. HT[V] data of the dipeptide systems with HT[V] data of the background solvent subtracted, data are shown over the course of gelation. Inserts show expanded spectra for the 250 – 350 nm region. Data collected on a Jasco J-715 spectropolarimeter at 21 °C in a 0.01 mm pathlength. (a) H-Nap-AA, (b) H-Nap-AV, (c) Br-Nap-AA, (d) Br-Nap-AV, (e) CN-Nap-AA, (f) CN-Nap-AV

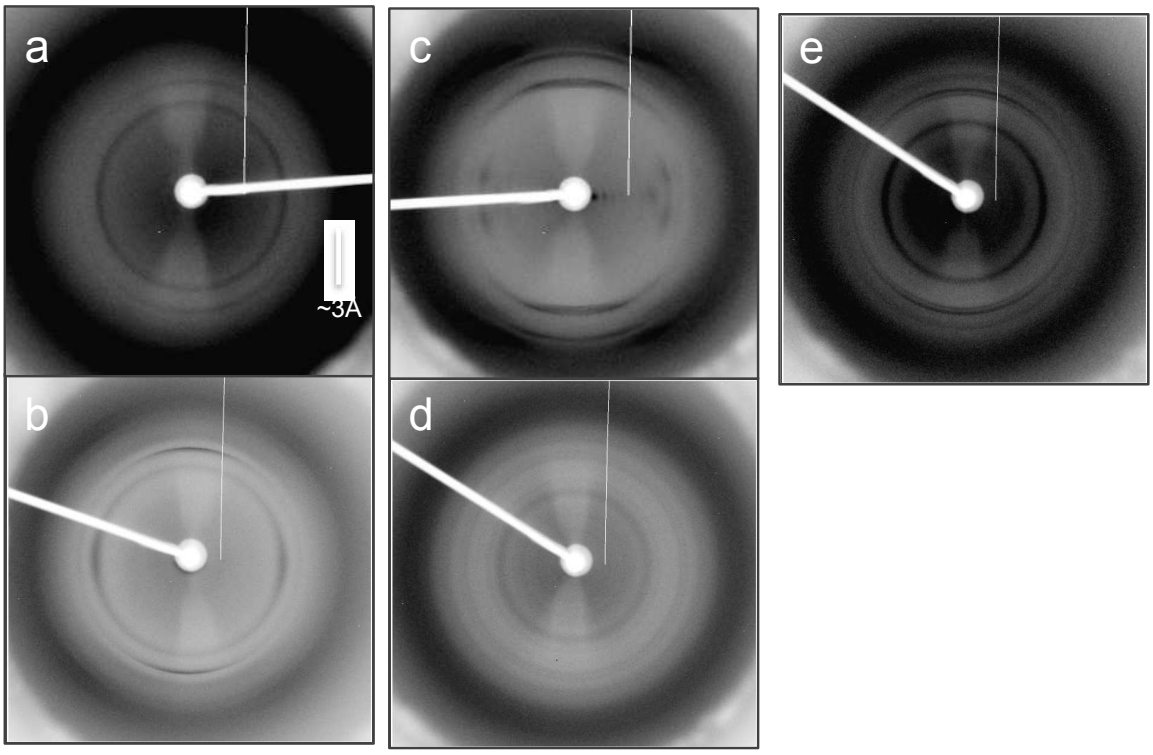

Figure S6. X-ray fibre diffraction data of the library (a) H-Nap-AA, (b) Br-Nap-AA, (c) Br-Nap-AV, (d) CN-Nap-AA, (e) CN-Nap-AV in the semi-hydrated states.

REFERENCES

(1) Rodger, A.; Norden, B. *Circular Chroism & Linear Dichroism*; OUP Oxford, 1997.